



# Temporal investigation of radionuclides and heavy metals in a coastal mining area at Ierissos Gulf, Greece

Filothei K. Pappa<sup>1,2</sup> · Christos Tsabaris<sup>1</sup> · Dionisis L. Patiris<sup>1</sup> · Georgios Eleftheriou<sup>1</sup> · Alexandra Ioannidou<sup>3</sup> · Effrosini G. Androulakaki<sup>1</sup> · Michael Kokkoris<sup>2</sup> · Roza Vlastou<sup>2</sup>

Received: 20 February 2019 / Accepted: 8 July 2019 / Published online: 22 July 2019  
© Springer-Verlag GmbH Germany, part of Springer Nature 2019

## Abstract

Vertical variations of radionuclides, trace metals, and major elements were determined in two sediment cores, which were collected in the marine environment of Ierissos Gulf near Stratonis's mining area. The enrichment factors (EFs) were also estimated and provided moderately severe to extremely severe enrichment for most trace elements and Mn, describing the anthropogenic influence in the gulf during the previous century. According to the applied dating models based on <sup>210</sup>Pb and <sup>137</sup>Cs, the effect in the marine sediment due to the exploitation of pyrite for the production of sulfuric acid during 1912–1920 was observed. Additionally, the decrease of mining activity during 1935–1945 due to the Second World War and the type of ore exploitation, the alteration of the exploited ores, and the construction and operation of Olympiada's floatation plant during 1950–1970 were identified. The end of tailing discharging into the marine environment during 1980–2010 was also noted.

**Keywords** Radionuclides and heavy metals · Marine sediment · Ierissos Gulf · Radiometric dating · Enrichment factor

## Introduction

Monitoring of radionuclides and metal contaminants in the marine environment is crucial for protection issues, as well as for studying environmental processes, especially in coastal areas where long-term industrial activities occur. Based on radiometric dating methods, sediment profiles have been extensively used to assess the accumulation and pollution of metals, to describe the environmental conditions of the past and to investigate the contamination history of different areas

(e.g., Valette-Silver 1993; Zeng and Wu 2009; Ferrand et al. 2012; Wang et al. 2015; Yao and Xue 2014, 2016; Grygar et al. 2016). Traditionally, sediment dating method is based on the combination of two radio-tracers, most commonly of <sup>210</sup>Pb and <sup>137</sup>Cs (Vaalgamaa and Korhola 2007; Ruiz-Fernandez and Hillaire-Marcel 2009; Szarlowicz et al. 2013; Baskaran et al. 2014). Although heavy metal and radionuclide concentrations in sediment cores have been studied in many regions such as streams/rivers (Wennrich et al. 2004; Pavlovic et al. 2005; Ferrand et al. 2012; Grygar et al. 2016), lagoons (Mejjad et al. 2018), and lakes (Noli and Tsamos 2018), there is lack of documented studies in the marine environment near mining areas (Pappa et al. 2018).

It has been noted that areas in the vicinity of mines are frequently subject to contamination and thus are comparatively more vulnerable (Zeng and Wu 2009; Szarlowicz et al. 2013; Wang et al. 2015; Yao and Xue 2014, 2016). The ecological impact due to mining sub-products releases in the environment, either from accidents (Riba et al. 2002) or from waste disposals (Panagopoulos et al. 2009; Wang et al. 2015; Pappa et al. 2016), is under investigation by environmental agencies and local communities. Furthermore, measurements of activity concentrations of natural radionuclides in coastal mining areas are highly requested to define baseline information for the sediment.

Responsible editor: Georg Steinhauser

**Electronic supplementary material** The online version of this article (<https://doi.org/10.1007/s11356-019-05921-5>) contains supplementary material, which is available to authorized users.

✉ Filothei K. Pappa  
fkpappa@hcmr.gr

<sup>1</sup> Institute of Oceanography, Hellenic Centre for Marine Research, 46.7 km Athens-Sounio Ave, 19013 Anavyssos, Greece

<sup>2</sup> Department of Physics, National Technical University of Athens, 15780 Zografou, Greece

<sup>3</sup> Nuclear Physics and Elementary Particle Physics Division  
Department of Physics, Aristotle University of Thessaloniki,  
54124 Thessaloniki, Greece

Over the last decades, an ongoing-mining area in Greece located at Stratoni, Ierissos Gulf, has been a subject of investigation concerning environmental contamination due to the mining activities and waste deposits including mine tailings, flotation tailings, metallurgical slags, waste rock, and pyrite concentrate stockpiles (Stamatis et al. 2002; Lazaridou-Dimitriadou et al. 2004; Hadjibiros et al. 2006; Kelepertsis et al. 2006; Kelepertzis et al. 2012). A more comprehensive study regarding the marine environment of Ierissos Gulf was held by Pappa et al. (2016, 2019), revealing the affected area in the coastal region due to waste disposals, as well as the enhanced values of metals and radionuclides compared with other aquatic environments of the area and the Mediterranean Sea. It is evident that the mining wastes are necessary to be studied regarding natural radioactivity (EC 2003) and heavy metal concentrations. In general, natural radioactivity occurs in the Earth's crust and activities related to the extraction and processing of ores can lead to enhanced levels of naturally occurring radioactive material in products, by-products, and wastes (Paiva et al. 2019). Thus, the study of radioisotopes present in the geological materials is necessary for radiological protection issues. Such a case is the Kassandra mining district, which is characterized by a great surface of granodiorite, and where the mining area of Stratoni is located (Gilg and Frei 1994). The content of natural radionuclides (U, Th, and K) in granodiorite of Stratoni has been studied by Persianis et al. (2010) and was found to have high concentrations. During the exploitation of the P.B.G. (Pyrite, Blende Galena) ores, part of the granodiorite is mined and which remains in the residuals of the mining process. Therefore, in a recent work, the content of radioactive elements was calculated in the products of Stratoni flotation plants (sulfide concentrates) and was found less than those in the granodiorite rock (Tzamos et al. 2019). However, until now, there are not enough data to provide information about the contamination levels of metals and radionuclides in the coastal environment of Stratoni, where the flotation residuals and mining wastes were discharged. For this reason, two sediment cores were collected from the marine environment of Ierissos Gulf, in vicinity with Stratoni mining area, to determine temporal variations of radionuclides and heavy metals.

The main objectives of this work are (a) to reconstruct historical events of sediment contamination and (b) to assess the concentrations of natural radionuclides and metals in the sediment.

## Materials and methods

### Study area and field work

Stratoni is located at the north part of Ierissos Gulf. It belongs to the mining area, known as Kassandra mining district

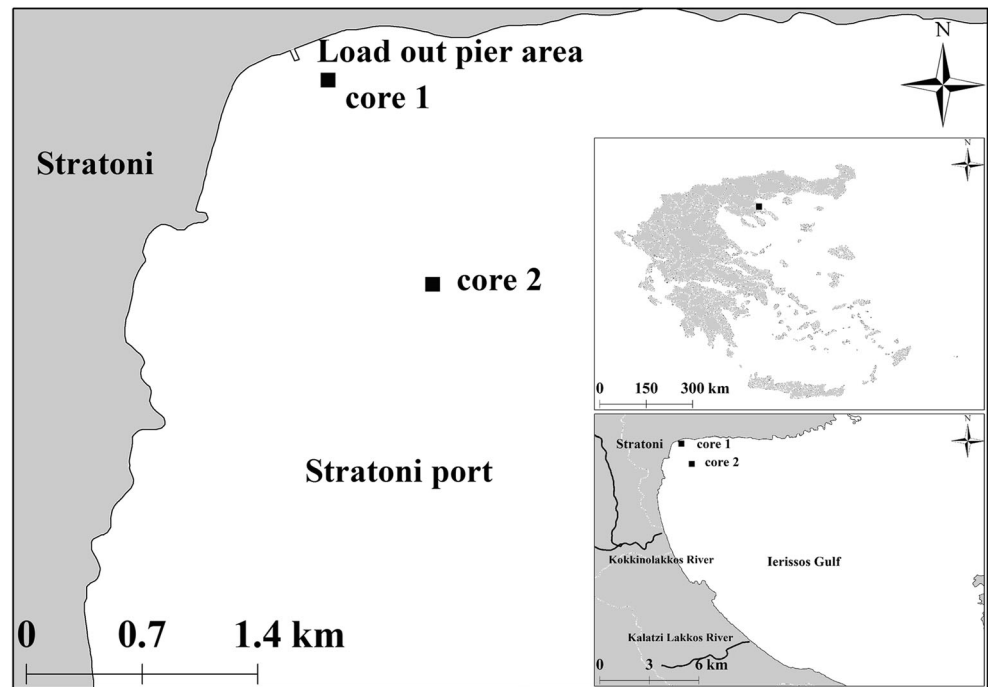
(Mavres Petres, Madem Lakkos, and Stratoniki deposits), and is characterized by polymetallic mineralization. The primary minerals in the area's ore deposits are pyrite ( $\text{FeS}_2$ ), sphalerite/zinc blende ( $\text{ZnS}$ ), and galena ( $\text{PbS}$ ), known as P.B.G., while secondary ones are arsenopyrite ( $\text{FeAsS}$ ), rhodochrosite ( $\text{MnCO}_3$ ), chalcopyrite ( $\text{CuFeS}_2$ ), bornite ( $\text{Cu}_5\text{FeS}_4$ ), and magnetite ( $\text{Fe}^{2+}\text{Fe}^{3+}_2\text{O}_4$ ) (Kelepertsis et al. 2006; Kelepertzis et al. 2012). Some of the gangue minerals are quartz ( $\text{SiO}_2$ ), rhodochrosite ( $\text{MnCO}_3$ ) and calcite ( $\text{CaCO}_3$ ). The streams of the drainage basin of Kassandra mining district discharge in the north part of Ierissos Gulf. In the same region are located the floatation plant and the load out pier area of Stratoni's mining industry.

Two campaigns of marine sample collection were held in June 2014 and in November 2015 at Ierissos Gulf at Chalkidiki Peninsula (North Greece). In the first campaign, a coastal core (core 1) was collected by a diver at 10.3 m depth and at 0.23 km distance from the shore (Lat.  $40^\circ 30.962' \text{N}$ , Lon.  $23^\circ 50.018' \text{E}$ ). In the second campaign, an offshore core (core 2) was collected by the crew of research vessel "AEGEAO" via a box corer at 58.8 m and at 1.35 km distance from the shore (Lat.  $40^\circ 30.295' \text{N}$ , Lon.  $23^\circ 50.360' \text{E}$ ). The maximum depth of the offshore core was chosen as the reference sample since exhibited the minimum observed concentration values for the studied radionuclides and trace metals. Therefore, it was considered as pre-mine deep sediment layer corresponding to background levels used for the enrichment factor and metal flux profile estimations. The map of the sampling points is showed in Fig. 1.

### Sample preparation

The bulk core samples were treated for radioactivity, trace metal, and the major element measurements, as well as for grain size distribution analysis at Hellenic Centre for Marine Research as described in Pappa et al. (2018). Prior to gamma-ray and XRF spectrometry, the sediment core was cut per 1 cm and the samples were treated by a standard procedure including drying, sieving, and pulverization, in order to achieve a homogeneous powder (IAEA 2003; Tsabaris et al. 2012). According to this procedure, the no-sediment (e.g., stones) and the gravel parts ( $> 2 \text{ mm}$ ) were extracted from the bulk sample. The remaining mass was dried and grounded. The produced powdered samples were placed in cylindrical containers per 1 cm or 2 cm depending on the available mass. The cylindrical containers were sealed for an appropriate period of time, so as secular equilibrium between  $^{226}\text{Ra}$  and  $^{214}\text{Pb}$  and  $^{214}\text{Bi}$  to be achieved. The used container was made by polyethylen and the samples were hermetically sealed. Moreover, the radioactive equilibrium was ensured by measuring the sealed samples in different periods of time. For the trace metal and major element determination, 5 g of the powdered sample were pressed in specific geometry and 0.6 g

**Fig. 1** The sampling stations of the sediment cores



were fused respectively, according to the methodology by Karageorgis et al. (2005).

## Analytical techniques

### Radionuclide and metal analysis

Activity concentration measurements of the core sediment samples were performed by means of gamma-ray spectrometry using two high-purity germanium (HPGe) detectors. Each detector had nominal relative efficiency of 50% and the measurements were performed at the Nuclear Laboratory of the Physics Department of National Technical University of Athens (NTUA) (Canberra GC5021) and at HCMR (ORTEC GEM-FX8530P4). The majority of the measurements were held at the NTUA laboratory, due to the limited availability of detection time at the HCMR laboratory. However, repetitive gamma-ray measurements were realized at HCMR, for the detection of the  $^{210}\text{Pb}$  peak at 45 keV as the thin carbon-fiber window of the HCMR detector allows this measurement. An intercomparison exercise followed between the two laboratories to ensure the consistency of the measurements and the results were found to be in good agreement within uncertainties for the energy range of 100–1500 keV. During all measurements, the cylindrical containers of the samples were placed directly on the detector's window and the acquisition time was set at 24 h for each sample. A lead shield was surrounding the detectors, in order to reduce the ambient gamma-ray background. The photopeak analysis was performed for natural radionuclides and  $^{137}\text{Cs}$ , using SPECTRW spectroscopy software package (Kalfas et al.

2016). The analyzed photopeaks and the methodology of the photopeak analysis are described in Patiris et al. (2016) and in supporting information document of Pappa et al. (2018). The necessary steps for activity concentration calculation (e.g., detectors' efficiency calibration, true coincidence summing effect corrections, and self-attenuation corrections) are described in Tsabaris et al. (2007); Patiris et al. (2016); and Pappa et al. (2016). The validation of radionuclide determination was verified via the analysis of the certified reference material IAEA-385. For all the measured radionuclides, the mean  $|z|$  score was calculated to be 1.1, while in all cases no outliers ( $|z| > 3$ ) were found. The uncertainty budget was determined taking into account the photopeak-counts statistical uncertainty, the intensity of the gamma-rays, the efficiency of the detector, and the sample mass. The calculated uncertainty includes the 95% of confidence level.

The adopted methodology for measuring trace metals and major elements in marine sediments by means of XRF spectrometry and the limit of determination are described in Karageorgis et al. (2005). In short, for the determination of the trace metal and major element concentration in the sediment samples, a Wavelength Dispersive XRF (WDXRF) system was used. The element identification and metal quantification were automatically deduced using the Panalytical ProTrace software. The XRF system stability determination and re-calibration was periodically checked and achieved using certified sediment standards (Karageorgis et al. 2005, 2009). The validation of metal determination was verified via the analysis of the certified reference material IAEA-458. For all the measured major elements and trace metals, the mean  $|z|$  score was calculated to be 0.05 and 0.6, respectively, while in

all cases no outliers ( $|z| > 3$ ) were found. The uncertainty budget was determined taking into account the laboratory reproducibility, the divergence between the measured and the assigned values of the certified materials, and the uncertainty of the assigned values (Pappa 2018). The XRF Laboratory is accredited according to ELOT EN ISO/IEC 17025. The calculated uncertainty includes the 95 % of confidence level.

### Dating analysis, contamination assessment, and metal flux calculations

The methodologies regarding the applied radiochronology techniques, the contamination assessment (enrichment factor (EF) and pollution load index (PLI)), and the metal flux (MF) calculation implemented in this work are described in detail in a previous work (Pappa et al. 2018). In brief, EF is defined as the normalization of metal concentration to a conservative element in the sample, as well as to a reference material free of any source of contamination. Similarly, PLI is defined as the normalization of the metal concentration in the sample to a reference sample for all the metals of interest. Additionally, MF is defined as the rate of the geochemical or industrial input of metals in the sediment. The dating method for the estimation of the sedimentation rate (SR) was performed on the collected sediment core 1 using the vertical profiles of the natural radionuclide  $^{210}\text{Pb}$  and artificial radionuclide  $^{137}\text{Cs}$  as described in Eleftheriou et al. (2018) and Pappa et al. (2018). According to Eleftheriou et al. (2018), the constant flux-constant sedimentation (CF:CS) model based on  $^{210}\text{Pb}$  can be satisfactorily applied in a wide range of environments. Thus, in this work, this model was utilized for the sedimentation rate estimation, where the excess  $^{210}\text{Pb}$  ( $^{210}\text{Pb}_{\text{ex}}$ ) was determined by the difference between measured  $^{210}\text{Pb}$  and  $^{226}\text{Ra}$ . The assumptions of the CF:CS model are described in detail in Eleftheriou et al. (2018).

Additionally, as mentioned in the previous work, the contamination assessment can be achieved by combining simplified and more detailed indices, such as pollution load index and enrichment factor, respectively. The first index (PLI) was applied in both cores (cores 1 and 2) in a conservative way, taking into consideration the elements of As, Cu, Pb, Zn, and Mn, which exhibited the highest concentrations among the studied elements. This approach is the first step to study an area so as to assess rapidly the contamination. On the other hand, EF is more detailed index and reveals the main contributors in the contamination. It depends from the establishment of the background (reference) value and the selection of the conservative metal for normalization. A recent detailed study is described in literature (Birch 2017) to establish the background value of metals (pre-anthropogenic concentrations) according to several empirical methods (e.g., use of global mean concentrations, pristine areas within the same ecosystem, pristine fluvial sediments, use of sedimentary cores of

high depth). The proposed method is to use background sample from the high depth of a sedimentary core (Birch 2017). Thus, in this work, the maximum depth of the offshore core (core 2) was selected as background sample since it is considered a pre-mine deep sediment layer within the same ecosystem of the study area, while the long-term mining operations (from ancient times until nowadays) at Stratoní port influenced the maximum depth of the coastal core (core 1). For consistency reasons, the concentrations of this background sample were also utilized in the PLI estimation. Additionally, in this work, all the major elements and the majority of trace metals showed variations in the sediment cores. Therefore, for the selection of the proper normalizing element, the methodology described by Karageorgis et al. (2009) was adopted. Based on this methodology, Al was selected as normalizing element, as it showed the minimum coefficient of variation ( $V$ ).

More adequate for the estimation of the EF and PLI indices are the deepest layers of an unaffected sediment core as mentioned above. However, a feasibility study estimated the EF of the background sample based on the concentrations of the continental crust. This approach is proposed not only for the verification of the correct selection of the background sample but also for providing EFs that can be compared in a global scale. Therefore, the EFs of the background sample (ecosystem) were estimated relatively to the shale of the continental crust (global) and were used for each metal as an indicator of the adequate selection of background sample. If this indicator ( $K$ ) is below 3, the selection of the background sample can be used as a reference since the anthropogenic influence is minor (Birch and Davies 2003). Otherwise, a new background sample has to be selected or another empirical/statistical method (Birch 2017) has to be applied for further data analysis. The used global mean elemental concentrations were those of As, Cu, Pb, Zn, Mn, and Al in the shale of the continental crust, exhibiting values of  $13 \mu\text{g g}^{-1}$ ,  $45 \mu\text{g g}^{-1}$ ,  $20 \mu\text{g g}^{-1}$ ,  $95 \mu\text{g g}^{-1}$ ,  $850 \mu\text{g g}^{-1}$ , and  $80 \times 10^3 \mu\text{g g}^{-1}$ , respectively (Wedepohl 1995).

A simplified equation (Eq. 1) is provided to reproduce the study-area representative enrichment ( $EF_{\text{ecosystem}}$ ) using the “global” enrichment factor ( $EF_{\text{global}}$ ), which are both calculated from EF equation (see Pappa et al. (2018)). The ratio of the two EFs ( $EF_{\text{global}}/EF_{\text{ecosystem}}$ ) represents the aforementioned indicator for the adequate selection of background sample.

$$K = \frac{EF_{\text{global}}}{EF_{\text{ecosystem}}} \Rightarrow EF_{\text{ecosystem}} = \frac{EF_{\text{global}}}{K} \quad (1)$$

Enrichment factor above a certain threshold indicates the level of contamination, which can be classified according to Birch and Davies (2003). Briefly, the EF classification can be expressed quantitatively as  $EF < 3$ ,  $3 \leq EF < 5$ ,  $5 \leq EF < 10$ ,  $10 \leq EF < 25$ ,  $25 \leq EF < 50$ , and  $EF \geq 50$ , to describe no or minor

enrichment, moderate enrichment, moderately severe enrichment, severe enrichment, very severe enrichment, and extremely severe enrichment, respectively. Furthermore, the class of enrichment according to Salomons and Forstner (1984) (based on the continental crust concentrations) is  $EF > 4$ , indicating other sources apart from weathering (e.g., anthropogenic).

Moreover, MF calculation was utilized for the evaluation of both geochemical and industrial input of metals into aquatic sediments. In the present study, as baseline elemental concentration was considered the one of the deepest sample of core 2. The excess metal flux ( $MF_i$ ) of core 1 was determined by subtracting the elemental concentration of the  $i$ th depth of core 1 from the elemental concentration of the deepest sample of core 2.

## Results

### Sedimentation rate

The sedimentation rate (SR) of core 1 was estimated using the  $^{137}\text{Cs}$  and  $^{210}\text{Pb}$  activity concentration profiles. The vertical profile of  $^{137}\text{Cs}$  activity concentration is depicted in Fig. 2a, along with the equation of  $^{137}\text{Cs}$ -peak maxima versus the historical nuclear incidents of nuclear tests in 1963 and the Chernobyl accident in 1986. The sedimentation rates utilizing independently the maxima of  $^{137}\text{Cs}$ , which correspond to the incidents of 1963 and 1986, were found  $(0.21 \pm 0.02) \text{ cm years}^{-1}$  and  $(0.24 \pm 0.01) \text{ cm years}^{-1}$ , respectively. The estimated sedimentation rates are consistent within uncertainties and the produced differences in sediment ages ranged from  $< 1$  to 16 years among the surface and the deepest layers of the core (110 years before), respectively. Thus, the mean value  $(0.23 \pm 0.01) \text{ cm years}^{-1}$  of these SRs was utilized for the validation of  $^{210}\text{Pb}$  radiometric model. The activity concentration profiles of  $^{210}\text{Pb}$  and  $^{226}\text{Ra}$  are shown in Fig. S11 (see Supporting Information document), where the exponential trend of  $^{210}\text{Pb}$  is evident verifying the assumption of the radiometric model. The activity concentration of the excess  $^{210}\text{Pb}$  versus depth is depicted in Fig. 2b. The uncertainties for  $^{137}\text{Cs}$  and  $^{210}\text{Pb}$  activity concentrations were 28% and 11%, respectively. Both methods revealed consistent sedimentation rates of  $(0.23 \pm 0.01) \text{ cm years}^{-1}$  for  $^{137}\text{Cs}$  and  $(0.26 \pm 0.06) \text{ cm years}^{-1}$  for  $^{210}\text{Pb}$ . The validation of  $^{210}\text{Pb}$  radiometric model was performed via  $^{137}\text{Cs}$  sedimentation model. The difference of the ages produced by the two calculated sedimentations rates was up to 10 years. The uncertainties of both sedimentation rates were estimated via the slope of the graphs (Fig. 2a, b) and include an age uncertainty ranging from  $< 1$  to 50 years for  $^{210}\text{Pb}$  and from  $< 1$  to 10 years for  $^{137}\text{Cs}$  among the surface and the deepest layers of the core (110 years before), respectively. Thus, the mean sedimentation rate was used in the reconstruction of historical levels of metals and radionuclides at Stratoni port (core 1), as discussed in “Historical events.” The SR determination was not performed

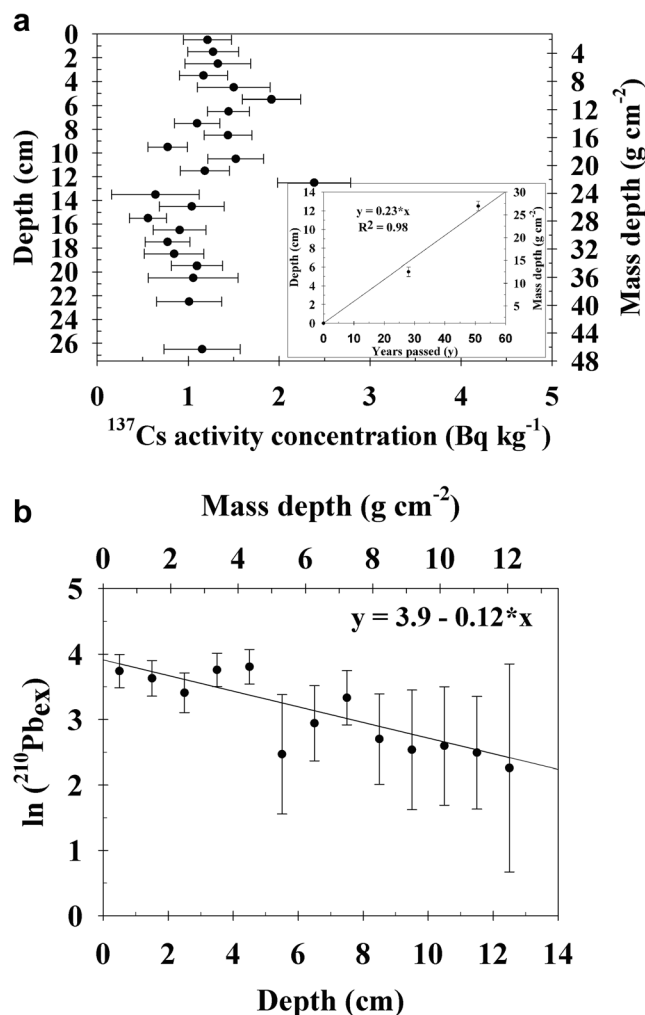


**Fig. 2** The sedimentation rate estimation based on  $^{137}\text{Cs}$  and  $^{210}\text{Pb}$  of core 1. **a** Sedimentation rate estimated from  $^{137}\text{Cs}$  activity concentration. **b** Sedimentation rate estimated from the unsupported  $^{210}\text{Pb}$  ( $^{210}\text{Pb}$  excess)

for core 2, as the little amount of the grounded powder of the sediment core resulted in using samples per 2 cm. This resolution arose the problem of concealing the  $^{210}\text{Pb}$  expected exponential decrease and the  $^{137}\text{Cs}$  signal.

### Grain size analysis

A rough estimation of the grain size distribution was performed in the samples. Subsamples of the bulk core sediments were split into sand and mud fractions by wet or/and dry sieving through a 63  $\mu\text{m}$  mesh. The sediment cores were separated into slices of 1 cm and grain size distribution analysis was performed. The results are shown in Fig. S1a for core 1 and Fig. S1b for core 2 (see Supporting Information document). Core 1 is characterized as muddy sand according to Folk’s classification (Folk 1974) and can be slightly divided in two parts: the upper part within 0–11 cm and the lower part within 12–27 cm. The upper part consists of 60–70% sand and

40–30% mud, and the lower part consists of 80% sand and 20% mud. Core 2 is characterized as sandy mud according to Folk's classification and can be also slightly divided into two parts: the upper within 0–12 cm and the lower one within 13–27 cm. The upper part consists of 60% sand and 40% mud, while the lower one consists of 70% sand and 30% mud.

### Radionuclide and metal concentrations

According to the radionuclide and metal profiles, the sediment core 1 was divided in two parts: the upper (0–11 cm) and a lower (12–27 cm), as mentioned above. The activity concentrations of natural radionuclides at the core sediments near the load out pier area (core 1) are depicted in Fig. S1 c, e in the Supporting Information document. The activity concentrations of natural radionuclides at the core sediments near the load out pier area (core 1) are depicted in Fig. S1 c, e in the Supporting Information document. The activity concentrations of  $^{228}\text{Ac}$ ,  $^{212}\text{Pb}$ ,  $^{212}\text{Bi}$ , and  $^{208}\text{Tl}$  exhibited similar values within uncertainties, verifying the secular equilibrium within  $^{232}\text{Th}$  decay series. Thus, in this work, the presented results of  $^{232}\text{Th}$  refer to the mean values of the aforementioned radionuclides. The values of  $^{226}\text{Ra}$ ,  $^{235}\text{U}$ ,  $^{232}\text{Th}$  series, and  $^{40}\text{K}$  ranged between  $75\text{--}120\text{ Bq kg}^{-1}$ ,  $4.8\text{--}13.4\text{ Bq kg}^{-1}$ ,  $30\text{--}40\text{ Bq kg}^{-1}$ , and  $570\text{--}860\text{ Bq kg}^{-1}$ , respectively, and their uncertainties were 3%, 13%, 12%, and 6%, respectively. At the upper part, the activity concentrations of  $^{226}\text{Ra}$ ,  $^{235}\text{U}$ , and  $^{40}\text{K}$  were 2 times less than those of the lower part of the core (see Fig. S1 c, e in the Supporting Information document). However, a homogeneous profile, within uncertainties, was observed for  $^{232}\text{Th}$  series, exhibiting a mean value of  $(30 \pm 3)\text{ Bq kg}^{-1}$ . The activity concentrations of  $^{226}\text{Ra}$ ,  $^{235}\text{U}$ ,  $^{232}\text{Th}$  series, and  $^{40}\text{K}$  of the offshore core ranged between  $(13\text{--}30)\text{ Bq kg}^{-1}$ ,  $(2.7\text{--}4.1)\text{ Bq kg}^{-1}$ ,  $(25\text{--}35)\text{ Bq kg}^{-1}$ , and  $(460\text{--}650)\text{ Bq kg}^{-1}$ , respectively, and are presented in Fig. S1 d, f (Supporting Information document). At the upper part of core 2 (0–11 cm),  $^{226}\text{Ra}$  and  $^{235}\text{U}$  exhibited higher values than in the lower part, while  $^{232}\text{Th}$  series were also characterized by a homogeneous profile. The observed difference among the vertical profiles of  $^{226}\text{Ra}/^{235}\text{U}$  and  $^{232}\text{Th}$  series indicates that  $^{226}\text{Ra}/^{235}\text{U}$  are affected by the mining activities occurring in the area. Additionally, the values of  $^{226}\text{Ra}$  and  $^{235}\text{U}$  in the offshore core are lower than those of the coastal core, indicating that the latter core was affected by the anthropogenic activities, which are depicted in its whole length. Nevertheless, the enhanced values of  $^{226}\text{Ra}$  and  $^{235}\text{U}$  in the upper part of the offshore core indicate that the influence of the anthropogenic activities reached the offshore—and not only the coastal—area of the gulf, for many years. However, this influence is only found in the first 12 cm and not only in the deeper layers.

The concentration profiles of trace metals (As, Zn, Cu, Pb) and major elements (Mn, Al, Fe) are shown in Fig. 3b–d and Fig. S1g–S1j in the Supporting Information document. High concentrations of As, Zn, Cu, and Pb were obtained in the sediment core 1 ranging between  $(1.4\text{--}2.2) \times 10^3\text{ }\mu\text{g g}^{-1}$ ,  $(2\text{--}6) \times 10^3\text{ }\mu\text{g g}^{-1}$ ,  $(100\text{--}250)\text{ }\mu\text{g g}^{-1}$ , and  $(2.5\text{--}4.0) \times 10^3$

$\mu\text{g g}^{-1}$ , respectively, and their uncertainties were 12.2%, 9.1%, 5.3%, and 4.6%, respectively. The maximum values were observed in the lower part of the core and were up to 3 times higher than those measured in the upper part. The only exception was the concentration of As, exhibiting a maximum concentration at 12 cm sediment depth and following a linear gradual decrease to the levels found in the upper core part. The Mn, Al, and Fe concentrations ranged between  $(4\text{--}12) \times 10^3\text{ }\mu\text{g g}^{-1}$ ,  $(40\text{--}60) \times 10^3\text{ }\mu\text{g g}^{-1}$ , and  $(70\text{--}85) \times 10^3\text{ }\mu\text{g g}^{-1}$ , respectively, and their uncertainties were 4.9%, 5%, and 5%, respectively. The maximum values of Fe, Al, and K were observed at 12–27 cm (lower part) of the core and were 20–30% higher than those obtained at 0–11 cm (upper part). However, the highest concentrations of Mn were obtained in the upper part of the core and those values were up to 4 times higher than those of the lower part.

The concentration profile of trace metals of core 2 is similar to those of  $^{226}\text{Ra}$  and  $^{235}\text{U}$ , wherein elevated values are observed in the first 12 cm, which decrease in deeper layers (Fig. 4). These elevated values cannot be only attributed to the fine grain fraction of core 2, as the sand-mud vertical distribution changes slightly between the upper part (0–12 cm) and the lower one (13–27 cm). The vertical distribution among the two cores indicates that both have been affected by the anthropogenic activities, wherein core 2 in a lesser extent, as shown by the one-order-of-magnitude lower values of trace metal concentrations comparing with core 1. These activities have affected the coastal area for many years, as shown by the high concentrations of trace metals in core 1. Additionally, this impact is evident in the offshore area (core 2), however for fewer years as indicated by the elevated values found only in the first 12 cm.

### Excess metal flux

The excess metal fluxes of core 1 were calculated for trace and major elements taking into account the satisfactory agreement of the sedimentation rates using the  $^{210}\text{Pb}$  and  $^{137}\text{Cs}$  dating methods. The profiles of the excess metal fluxes are depicted in Fig. 3b–d and Fig. S1g–S1j in the Supporting Information document, together with the trace/major metal profile. The excess fluxes of Al and Fe ranged from  $(0\text{ to }5) \times 10^3\text{ }\mu\text{g years}^{-1}\text{ cm}^{-2}$  and from  $(14\text{ to }20) \times 10^3\text{ }\mu\text{g years}^{-1}\text{ cm}^{-2}$ , respectively. The maximum values of the Fe excess flux were obtained at 12 cm and 20 cm depth, while the maximum values of the Al one at the lower part of the core (11–27 cm). The Mn excess flux ranged from  $(1.4\text{ to }3.5) \times 10^3\text{ }\mu\text{g years}^{-1}\text{ cm}^{-2}$ , and the maximum values were observed at the upper part of the core (0–10 cm). The As excess flux ranged from  $350\text{ to }650\text{ }\mu\text{g years}^{-1}\text{ cm}^{-2}$  and two local maxima were obtained at 12 cm ( $650\text{ }\mu\text{g years}^{-1}\text{ cm}^{-2}$ ) and at 20 cm ( $550\text{ }\mu\text{g years}^{-1}\text{ cm}^{-2}$ ). The Cu and Pb metal fluxes ranged from  $(30\text{ to }95)\text{ }\mu\text{g years}^{-1}\text{ cm}^{-2}$  and from  $(0.4\text{ to }2) \times 10^3\text{ }\mu\text{g years}^{-1}$

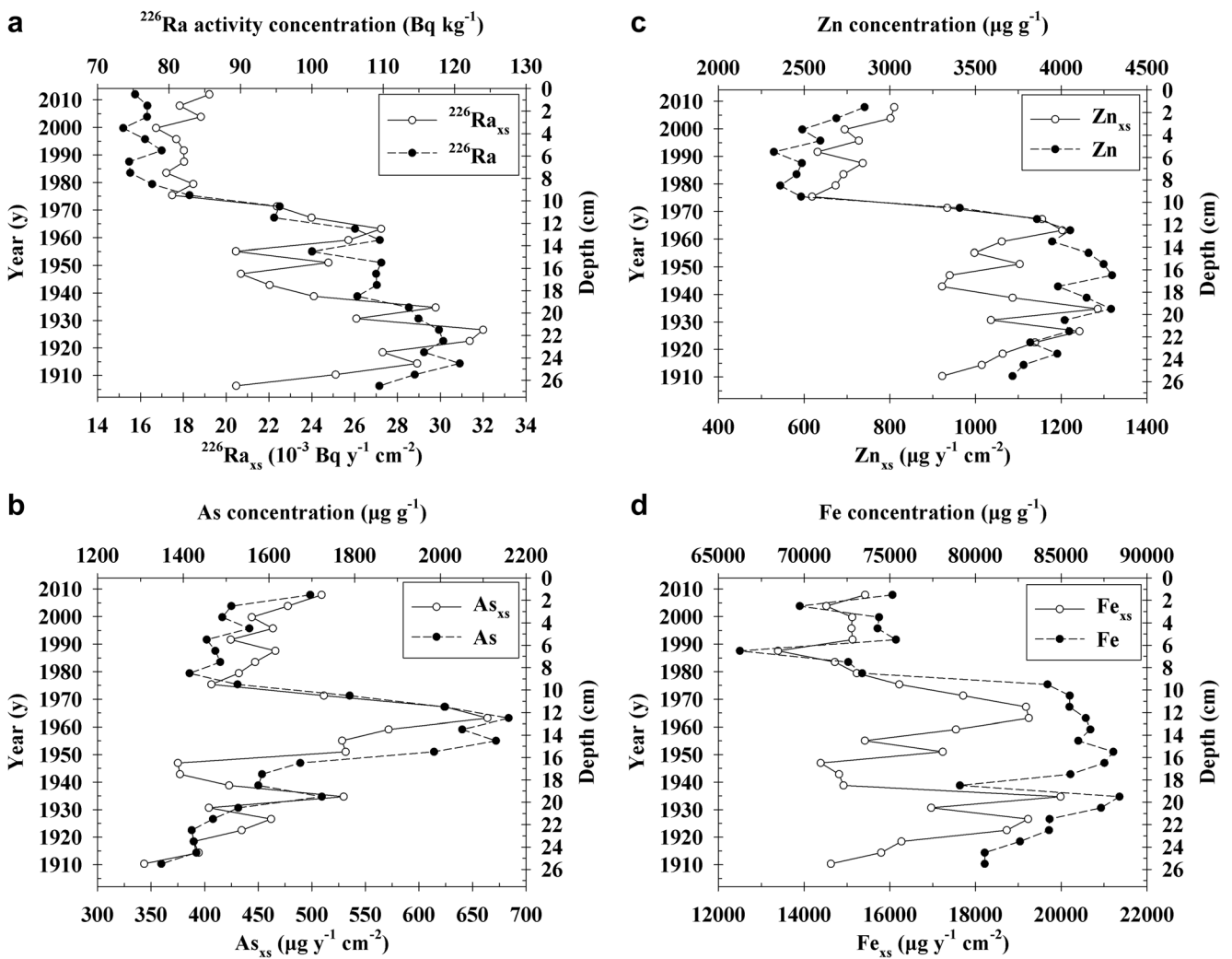
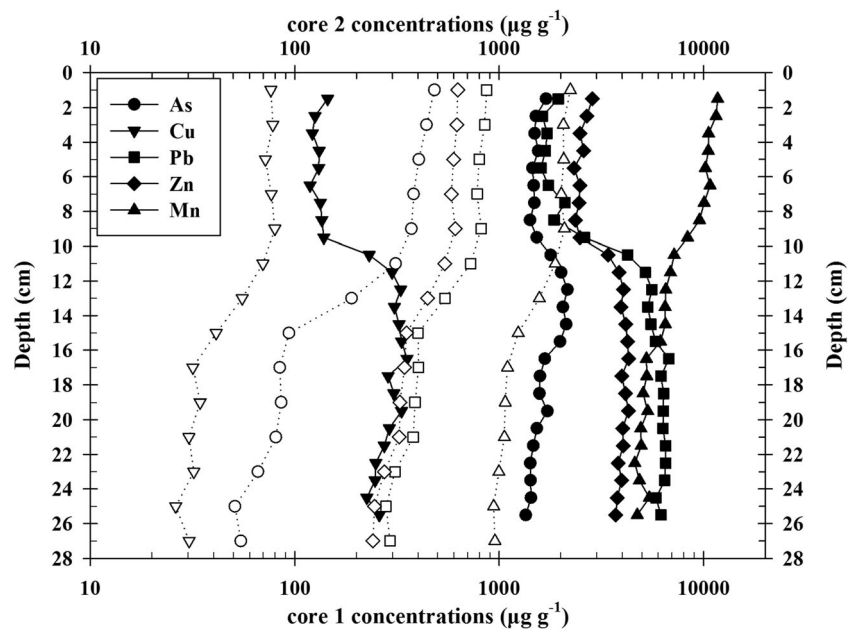


**Fig. 3** The concentrations and excess metal fluxes of  $^{226}\text{Ra}$ , As, Zn, and Fe. **a** Excess metal flux and concentration of  $^{226}\text{Ra}$ . **b** Excess metal flux and concentration of As. **c** Excess metal flux and concentration of Zn. **d** Excess metal flux and concentration of Fe

**Fig. 4** The metal concentrations of the coastal (core 1-black markers) and offshore (core 2-white markers) cores at Stratoní port



$\text{cm}^{-2}$ , respectively. For both metal flux profiles, the maximum values were obtained in the lower part of the core (11–27 cm). The metal flux of Zn ranged from  $(0.6 \text{ to } 1.2) \times 10^3 \mu\text{g years}^{-1} \text{ cm}^{-2}$  and as in the cases of Fe and As two local maxima were observed at 12 cm and 20 cm.

The excess metal flux was also calculated for the long-lived natural radionuclides, as described in Pappa et al. (2018) and the results are depicted in Fig. 3a and S1k (in the Supplementary Information document). The metal flux values of  $^{226}\text{Ra}$  ( $^{226}\text{Ra}_{\text{xs}}$ ) ranged from  $(18 \text{ to } 32) \times 10^{-3} \text{ Bq years}^{-1} \text{ cm}^{-2}$ , where the low values were observed in the upper part of the core (0–10 cm). Two local maxima (as in Fe, As, and Zn excess metal profiles) were also obtained at 12 cm and 20 cm. The excess metal flux of  $^{235}\text{U}$  ( $^{235}\text{U}_{\text{xs}}$ ) ranged from  $(0.3 \text{ to } 2.7) \times 10^{-3} \text{ Bq years}^{-1} \text{ cm}^{-2}$ , and two slightly distinct local maxima could be observed at 14 cm and 21 cm, as in the  $^{226}\text{Ra}$  excess flux profile.

## Discussion

### Comparison with information values

In order to provide the historical trends of contamination, the results were analyzed according to the concentration trends with respect to the depth of the core 1. In the previous work of Pappa et al. (2016), the surficial concentrations of  $^{226}\text{Ra}$  in Stratoni area were found higher than those of coastal areas of Mediterranean Sea. Similar results can be observed by comparing the activity concentrations of  $^{226}\text{Ra}$  measured in the coastal core (core 1) of the present work with those obtained in sediment cores of the Mediterranean Sea (Bersanti et al. 2011). Additionally, the comparison of  $^{226}\text{Ra}$  concentrations in the soil and the sediment is not adequate due to the solubility of  $^{226}\text{Ra}$  in the marine environment; however, such a comparison can be accepted indicatively. Thus, the concentrations of  $^{226}\text{Ra}$  and  $^{40}\text{K}$  in the upper part (0–11 cm) of the core were up to 2 and 1.5 times higher than the world median values of  $^{226}\text{Ra}$  and  $^{40}\text{K}$  in the soil (UNSCEAR 2000), respectively (Table 1). The concentration of  $^{226}\text{Ra}$  in the lower part (12–27 cm) of the core was up to 3 times higher, while of  $^{40}\text{K}$  was 93% higher than the world median. The  $^{226}\text{Ra}$  concentrations of core 2 were similar or lower than those of the world median, while  $^{40}\text{K}$  exhibited also similar or higher (up to 60%) values than those of  $^{40}\text{K}$  in soil. The  $^{226}\text{Ra}$  concentrations of cores 1 and 2 were 2 times higher and similar to or lower than the  $^{226}\text{Ra}$  values measured in Stratoni's granitoids (Papadopoulos et al. 2013), respectively, indicating a  $^{226}\text{Ra}$  enrichment in core 1 due to mining activities. The  $^{232}\text{Th}$  series concentration in both cores was similar to the world median value obtained in the soil and 4 times lower than those obtained in Stratoni's granitoids, indicating that the radionuclides of  $^{232}\text{Th}$  series was not affected by the mining activities.

The concentrations of As, Pb, Zn, and Mn in the upper part of core 1 were up to 45, 15, 6, and 9 times higher than the sediment quality guidelines proposed by national organizations (USEPA 2000; ANZECC 2000; OMEE 1993), respectively (Table 1). Some of the numerous developed SQGs, such as PEC, ISQG, and PEL, have been adopted by regulatory agencies and are recommended for screening reasons (Burton 2002). The sediment quality guidelines (SQGs) established by the aforementioned national organizations, reflect the effect in the organisms living in the sediment. In this work, the upper limits of SQGs were utilized. Metal concentrations above SQGs indicate a heavily polluted area with expected adverse biological effects and a need for further testing of the contamination. The concentration of Cu in the upper part of the core was in the same level as these guidelines. The As and Mn profiles in the lower part of the core can be further divided in two additional areas: 12–16 cm and 17–27 cm. The concentrations of As and Mn at the 12–16 cm depth were found up to 64 and 6 times higher, while at the 17–27 cm depth, they were found up to 45 and 5 times higher than the guidelines, respectively. The concentrations of Pb and Zn in the lower part (12–27 cm) of the core reach up to 47 and 6 times higher than the sediment quality guidelines, while the concentration of Cu was in the same level with these values. Moreover, the concentrations of As, Pb, Zn, and Mn in the upper part (0–12 cm) of core 2 were up to 15, 7, 1.4, and 2 times higher than the sediment quality guidelines proposed by national organizations. On the other hand, these metals exhibited values lower than the sediment quality guidelines in the deeper layers, indicating non-affected layers due to the mining activities. The concentration of Cu in the whole core was lower than those guidelines. The elevated values of core 1 and core 2, compared with sediment quality guidelines, reveal also the most affected area of Ierissos Gulf, to be the one near the load out pier area (core 1).

### Historical events

The maximum values of natural radionuclides ( $^{226}\text{Ra}$ ,  $^{235}\text{U}$ ,  $^{40}\text{K}$ ), trace elements (Cu, Pb, Zn), and major elements (Al, Fe) were observed from 1908 to 1970 (core's lower part 12–27 cm). During that period, the mixed sulfide–manganese ores exploitation was held mainly by the Hellenic Chemical Products and Fertilizers Company (AEEHPL). The main ores that were exploited were pyrite ( $\text{FeS}_2$ ), sphalerite ( $\text{ZnS}$ ), and galena ( $\text{PbS}$ ), known as P.B.G. According to the trend of the excess mass fluxes of Fe ( $\text{Fe}_{\text{xs}}$ ), As ( $\text{As}_{\text{xs}}$ ), Zn ( $\text{Zn}_{\text{xs}}$ ), and  $^{226}\text{Ra}$  ( $^{226}\text{Ra}_{\text{xs}}$ ) (see Fig. 3a–d), five operational periods are observed: (a) 1912–1920, (b) 1920–1935, (c) 1935–1945, (d) 1950–1970, and (e) 1983–2014. The vertical distribution of mass fluxes in combination with the dating model resolved more efficiently (compared to metal concentrations) the plant operation periods.



**Table 1** Radionuclide concentrations of present work and world median of soil, as well as metal concentrations of this work, the shale of the continental crust, and metal guideline concentrations in sediments

Activity concentration (Bq kg <sup>-1</sup> )		<sup>226</sup> Ra	<sup>232</sup> Th*	<sup>235</sup> U	<sup>40</sup> K	<sup>137</sup> Cs	
Core 1	Min	75	30	4.8	570	0.6	(Present work)
	Max	120	40	13.4	860	2.4	
Core 2	Min	13	25	2.7	460	0.6	
	Max	30	35	4.1	650	4.7	
World median	Soil	35	30	–	400	–	(UNSCEAR 2000)
Metal concentrations (µg g <sup>-1</sup> )		As	Cu	Pb	Zn	Mn	
Core 1	Min	1400	120	1600	2300	4600	(Present work)
	Max	2200	350	6800	4300	12000	
Core 2	Min	54	80	280	240	940	
	Max	480	30	870	630	2230	
Shale		13	45	20	95	850	(Wedepohl 1995)
Sediment quality guidelines (µg g <sup>-1</sup> )							
PEC		33	149	128	459	–	(USEPA 2000)
ISQG	High	70	270	220	410	–	(ANZECC 2000)
SEL		33	110	250	820	1100	(OMEE 1993)

\*The activity concentrations of <sup>232</sup>Th correspond to the activity concentrations of <sup>228</sup>Ac, <sup>212</sup>Pb, <sup>212</sup>Bi, and <sup>208</sup>Tl, which exhibited similar values within uncertainties, verifying the secular equilibrium within <sup>232</sup>Th decay series.

PEC probable effect concentrations, ISQG interim sediment quality guidelines, SEL severe effect level

In 1912, the AEEHPL company bought Kasandra mines for the exploitation of pyrite (FeS<sub>2</sub>) of the Madem Lakkos deposit, so as to produce sulfuric acid. Almost simultaneously with the exploitation of FeS<sub>2</sub> began the P.B.G. exploitation during 1920–1935. During this period, an increment is observed in the profiles of Fe and As concentrations and mass fluxes, indicating a waste disposal of pyrite (FeS<sub>2</sub>) and arsenopyrite (FeAsS). The pyrite disposal was correlated to the efficiency of the used ore-separation method. Additionally, the P.B.G. ores were characterized by low percentage of As in the form of

secondary ores (arsenopyrite). Arsenopyrite has similar chemical characteristics with pyrite, which leads to its disposal during the separation method. Moreover, the increment of Cu and—in a lesser extent—Pb observed in their mass flux profiles during 1920–1935 may be attributed to the bad ore-separation efficiency, as part of them was disposed with the pyrite wastes and another one with the P.B.G wastes. The low Mn concentrations and mass fluxes during the same period indicate the exploitation of pure P.B.G. ores free from impurities such as rhodochrosite (MnCO<sub>3</sub>), while the elevated <sup>226</sup>Ra concentrations and mass fluxes may be attributed to Stratoni’s granitoids hosting the P.B.G. ores and characterized by secondary uranium minerals (Persianis et al. 2010; Papadopoulos et al. 2013).

In most profiles of radionuclide and metal concentration and mass fluxes (Fig. 3a–d and S1g–S1k in the Supporting Information document), especially in those of As, Fe, Zn, and <sup>226</sup>Ra, a local minimum is observed during 1935–1945, which reflects the impact to the mining activities due to the Second World War. From 1950 until 1970, the As concentration is further increasing, indicating either an alteration of the floatation method so as to have better efficiency in the P.B.G. ore recovery or exploitation of P.B.G. minerals characterized by higher percentage of As. The alteration of the floatation method during 1950–1970 was a result of abandoning the use of FeS<sub>2</sub> as the main material for the AEEHPL company to produce sulfuric acid. Thus, in the same period, a local maximum is observed in the Fe mass flux profile, with less values than those during

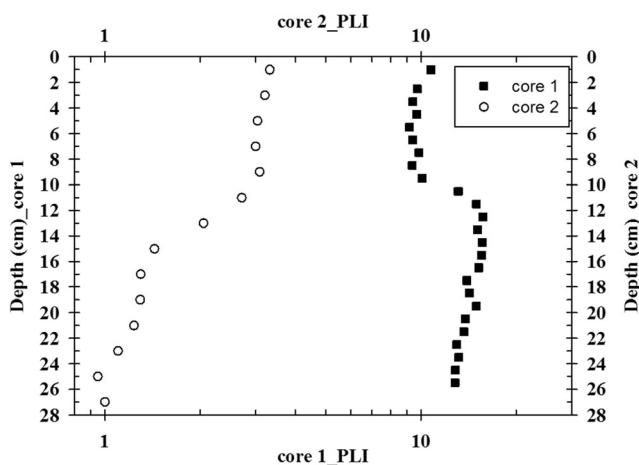
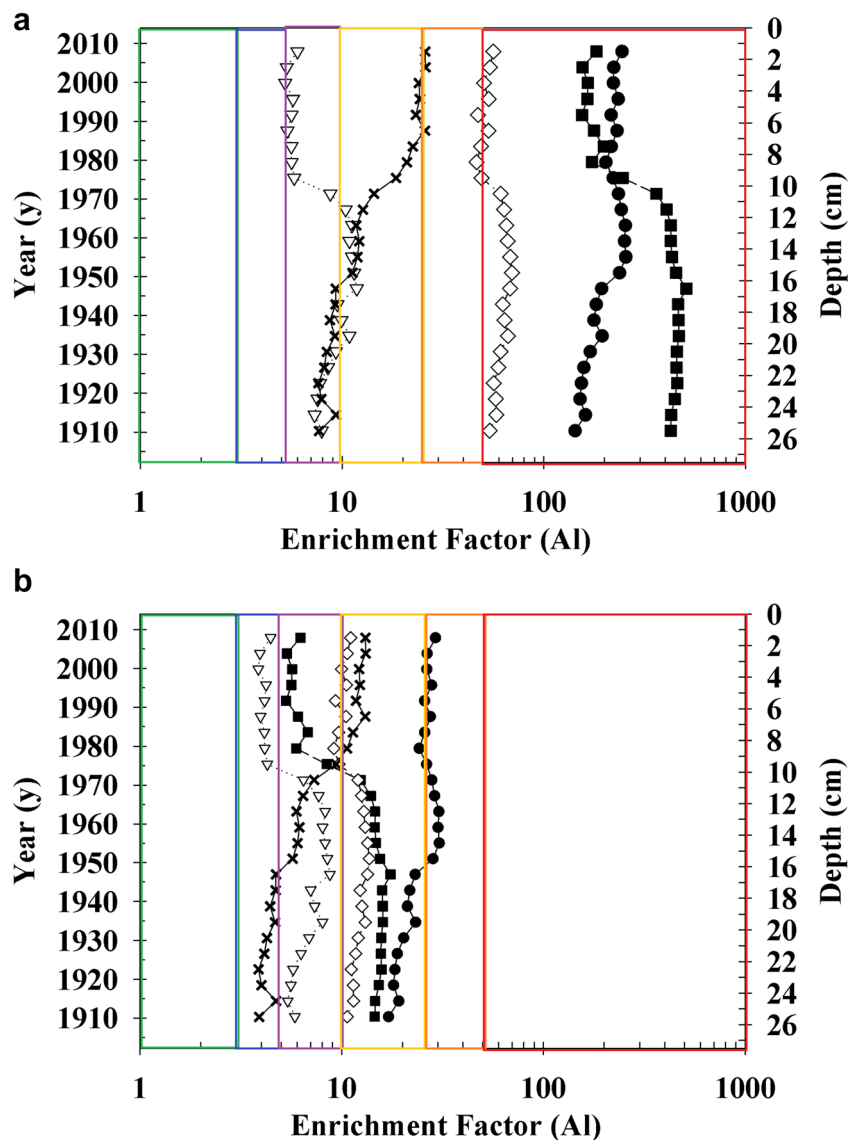


**Fig. 5** The PLI profiles of the coastal (core 1) and the offshore (core 2) cores at Stratoni port

**Fig. 6** The enrichment factor (EF) profiles of As, Cu, Zn, Pb, and Mn of the coastal core (core1) at Stratoni port, where Al was utilized as conservative element. The classification of the contamination is described by colors where green represents no or minor enrichment ( $EF < 3$ ), blue moderate enrichment ( $3 \leq EF < 5$ ), purple moderately severe enrichment ( $5 \leq EF < 10$ ), yellow severe enrichment ( $10 \leq EF < 25$ ), orange very severe enrichment ( $25 \leq EF < 50$ ), and the red extremely severe enrichment ( $EF \geq 50$ ). **a** For the estimation of the EF profiles, the elemental concentrations of the shale of the continental crust (Wedepohl 1995) were used as background values. **b** For the estimation of the EF profiles, the elemental concentrations of the deepest layer of core 2 were used as background values. This layer is assumed unaffected by the mining activities as it represents the period before the extensive mining in the area



1920–1935. The lower  $Fe_{xs}$  peak during 1950–1970 compared with the period of 1920–1935 may also reflect the exploitation of Mavres Petres deposit, instead of Madem Lakkos. Mavres Petres deposit is characterized by P.B.G. minerals with lower Fe percentage comparing with Madem Lakkos. For the same period, the lower values of  $^{226}Ra$  concentration and mass fluxes may be attributed to the location of the P.B.G. minerals. During 1950–1970, the P.B.G. ores were further away from the granitoids, than the period of 1920–1935, indicating the presence of smaller quantities of granitoids in the mining wastes.

The decrement of As during 1970–1975 may represent the storage of arsenopyrite, which was hosted in P.B.G. minerals. This type of arsenopyrite was enriched in As, thus during ore-separation, it was not disposed in the marine environment but it was sent away and was further exploited at Olympiada's newly-built flotation plant. At Olympiada's flotation plant,

arsenopyrite enriched in As was exploited, as in this type of mineral the percentage of Au being hosted was greater. Thus, at Stratoni's flotation plant, there were remaining arsenopyrite wastes with low percentage of As. During 1983–2014, in all concentration and mass flux profiles (except from those of Mn), the lowest values are observed. These minima reveal the cessation of tailing discharge into the marine environment (Kelepertzis 2013). Moreover, the decreasing concentrations and mass fluxes of Al from 1920 until 1970 may reveal the location of the exploited P.B.G. ores. In the beginning of the P.B.G. exploitation (1920–1935), the ores were located near to granitoids and pegmatite veins, which are characterized with high concentrations of Al, while later (1950–1970) the exploited P.B.G. were located further away than the pegmatite veins. Moreover, the maximum values of Mn concentration and mass flux were obtained during 1983–2014 and are

correlated with the transport processes in the coastal environment. Mn is present in Kassandra deposits, in the form of rhodochrosite ( $\text{MnCO}_3$ ), which is light and when disposed in the coastal environment, it is transported due to the wave movements. Additionally, the different type of tailing discharges can be probably described by the mud content of the sediment core 1 (see Fig. S1a of the Supporting Information document). It is clearly seen that after 1965, the mud content reaches the maximum value (up to 40%).

### Pollution load index

As discussed in “Radionuclide and metal concentrations,” the upper part (0–12 cm) of the offshore core (core 2) may have been affected by the anthropogenic activities, however in a lesser extent comparing to the coastal core (core 1). In order to assess the depth of contamination of both cores, the PLI index was calculated. This index is a simplified one and it includes the concentrations of the metals of interest normalized to a background site. Nevertheless, it does not take into consideration the grain size effect. In this work, a conservative approach was attempted, where the metals (trace and Mn) with the highest concentrations were utilized in the production of the PLI profiles, as shown in Fig. 5. Taking into account the classification by Tomlinson et al. (1980), both cores are contaminated in the whole length ( $\text{PLI} > 1$ ). However, in this work, PLI below 2 can be assumed that represents unaffected core depths from the mining activities, meaning the deep layers of core 2 (13–27 cm) are not contaminated. This assumption can be established to the fact that the PLI calculation was utilized conservatively, the offshore core exhibited one-order-of-magnitude lower PLI values comparing to the coastal core and the upper part (0–12 cm) of the offshore core received PLI values above 4, while the deeper part exhibited PLI values below 2.

### Enrichment factors

The enrichment factor (EF) profiles of heavy metals (As, Cu, Pb, Zn, and Mn) estimated for the sediment core collected at the load out pier area (core 1) are depicted at Fig. 6. The calculated EFs using as reference concentrations those of the continental shale are depicted in Fig. 6a. According to Birch and Davies (2003), the whole sediment core (upper and lower parts) is characterized as extremely severely enriched ( $\text{EF} > 50$ ) in As, Pb, and Zn. The upper part (0–11 cm) was severely enriched in Mn and moderately severely enriched in Cu, while the lower part (12–27 cm) of the core was mainly moderately severely enriched in Cu and Mn.

The calculated EFs using as reference concentrations those found deep pre-mine layer of core 2 are depicted in Fig 6b. According to Birch and Davies (2003), the upper part of the core was moderately, moderately severely, severely, and very

severely enriched in Cu, Pb, Zn and Mn, and As, respectively. The lower part of the core was moderately, moderately severely, and severely enriched in Mn, Cu and As, and Pb and Zn, respectively.

Concerning the classification of historical trends, a difference was observed regarding the used reference values of the EF estimation (global, ecosystem). The order of the enrichment according to the  $\text{EF}_{\text{global}}$  profile was  $\text{Pb} > \text{As} > \text{Zn} > \text{Mn} > \text{Cu}$  (Fig. 6a), while this order changed according to the  $\text{EF}_{\text{ecosystem}}$  profile as  $\text{As} > \text{Zn} \geq \text{Pb} > \text{Mn} > \text{Cu}$  (Fig. 6b). Only a slight change for the classification of Cu and Mn enrichment in the sediment core 1 was observed, for example, the sediment core was characterized as moderately severely enriched in Cu when using the global value, while it was characterized as moderately enriched in Cu when using the ecosystem value. However, the classification of As, Zn, and Pb in the sediment core altered, because the K value of these metals was above 3. Although  $\text{EF} > 4$  describes contamination, this difference in the classification indicates that the use of global continental crust data might not be representative for this specific area, as it represents a rough estimation and it should be used with caution and only for comparison reasons in global aspect. However, for the future, a deeper layer of a more distant offshore sample could be utilized to verify the EF classification of this work, based on the ecosystem background.

## Summary and conclusions

In the present study, the temporal variation of radionuclides ( $^{226}\text{Ra}$ ,  $^{40}\text{K}$ ,  $^{235}\text{U}$ ,  $^{232}\text{Th}$  series), trace metals (As, Cu, Pb, Zn), and major elements (Fe, Al, Mn) were obtained in Ierissos Gulf, Chalkidiki. The natural radionuclide, trace element, and Mn concentrations in core 1 sediments were well above the world median for soil (UNSCEAR 2000) (except for  $^{232}\text{Th}$  series) and national organization guidelines (USEPA 2000; ANZECC 2000; OMEE 1993) (except for Cu), respectively. The natural radionuclides determined in the offshore core (core 2) exhibited similar or lower values of the world median for soil, indicating an anthropogenic impact in the offshore area in a lesser extent in the first 12 cm. The similar homogeneous vertical distribution of  $^{232}\text{Th}$  series in the coastal and offshore core points out that this radionuclide is not affected by the mining activities.

The pollution load index indicated that also the metal contamination reached the offshore part (until 12 cm depth). The enrichment factor revealed severe to extremely severe enrichment during the previous century according to the analysis of the sediment core (coastal core). The order of the enrichment according to the  $\text{EF}_{\text{ecosystem}}$  was  $\text{As} > \text{Zn} \geq \text{Pb} > \text{Mn} > \text{Cu}$  for core 1 sediments, respectively.

The dating method was combined with the mass flux vertical distribution of core 1 in order to identify the historical trends of past contamination, taking into account the mining activity during the last century. The applied method reconstructed the mine operation periods from 1908–2014. The exploitation of pyrite for the production of sulfuric acid during 1912–1920, the decrease of mining activity during 1935–1945 due to the Second World War, the type of ore exploitation, the alteration of the exploited ores, and the construction and operation of Olympiada's floatation plant during 1950–1970; and the cessation of tailing discharging into the marine environment during 1980–2010 were identified. The determination of the mass fluxes and the enrichment factors for the trace metals proved that the Stratoni port and its adjacent area are highly affected from the mining activity that took place during the last century.

This work highlights the need of continuous and/or routine monitoring for environmental control of Ierissos Gulf and understanding the transport processes (spatially and temporally). Additionally, the need for the study of radionuclides and metals in other matrices (e.g., water, biota) in the marine area arises.

**Acknowledgments** Mrs. F.K. Pappa would like to acknowledge A.G. Leventis Foundation for the financial support of her PhD thesis, as well as Mr. Costas Papathanasiou for the fruitful discussions regarding the interpretation of the metal and metal flux profiles in the historical reconstruction section. Mrs. F.K. Pappa would also like to thank Mr. K. Sarantakos for the discussions regarding the classification of the metal enrichment into the sediment. The crew of the R/V AEGEAO is also acknowledged for providing samples from the offshore part of Ierissos Gulf.

## References

- Australian and New Zealand Environment and Conservation Council (ANZECC) (2000) Australian and New Zealand guidelines for fresh and marine water quality. National Water Quality Management Strategy, paper No 4, Vol. 2, chapter 8
- Baskaran M, Nix J, Kuyper C, Karunakara N (2014) Problems with the dating of sediment core using excess  $^{210}\text{Pb}$  in a freshwater system impacted by large scale watershed changes. *J Environ Radioact* 138: 355–363. <https://doi.org/10.1016/j.jenvrad.2014.07.006>
- Bersanti M, Delbono I, Schirone A, Langone L, Miserochi S, Salvi S, Delfanti R (2011) Sediment reworking rates in deep sediments of the Mediterranean Sea. *Sci Total Environ* 409:2959–2970. <https://doi.org/10.1016/j.scitotenv.2011.04.025>
- Birch GF (2017) Determination of sediment metal background concentrations and enrichment in marine environments – a critical review. *Sci Total Environ* 580:813–831. <https://doi.org/10.1016/j.scitotenv.2016.12.028>
- Birch GF, Davies K (2003) A scheme for assessing human impacts on coastal aquatic environments using sediments. In: Coastal GIS, Woodcoffe CD and Furness RA (eds) Wollongong University Papers in Center for Maritime Policy, 14, Australia, pp 371–380
- Burton GA (2002) Sediment quality criteria in use around the world. *Limnology* 3:65–76. <https://doi.org/10.1007/s102010200008>
- Eleftheriou G, Tsabaris C, Papageorgiou DK, Patiris DL, Androulakaki E, Pappa FK (2018) Radiometric dating of sediment cores from aquatic environments of north-east Mediterranean. *J Radioanal Nucl Chem* 316:655–671. <https://doi.org/10.1007/s10967-018-5802-8>
- European Commission (EC) (2003) Effluent and dose control from European Union NORM industries — assessment of current situation and proposal for a harmonized community approach, Radiation Protection 135, Office for Official Publications of the European Communities, Luxembourg
- Ferrand E, Eyrolle F, Radakovitch O, Provansal M, Dufour S, Vella C, Raccasi G, Gurriaran R (2012) Historical levels of heavy metals and artificial radionuclides reconstructed from overbank sediment records in lower Rhone River (South-East France). *Geochim Cosmochim Acta* 82:163–182. <https://doi.org/10.1016/j.gca.2011.11.023>
- Folk RL (1974) Petrology of the Sedimentary Rocks. Hemphill Publishing Company, Austin, p 182
- Gilg HA, Frei R (1994) Chronology of magmatism and mineralization in the Kassandra mining area, Greece: the potentials and limitations of dating hydrothermal illites. *Geochim Cosmochim Acta* 58:2107–2122
- Grygar TM, Elznicova J, Kiss T, Smith HG (2016) Using sedimentary archives to reconstruct pollution history and sediment provenance: the Ohre River, Czech Republic. *Catena* 144:109–129. <https://doi.org/10.1016/j.catena.2016.05.004>
- Hadjibiros K, Mantziaras ID, Sakellariadis DG, Giannakidou C, Katsiri A (2006) Pollution risk assessment from European mining sites and preliminary results from tailings dams in Greece. Proceedings of the 8th International Conference: Protection and Restoration of the Environment, 3–7 July 2006, Crete, Greece.
- International Atomic Energy Agency (IAEA) (2003) Collection and Preparation of Bottom Sediment Samples for Analysis of Radionuclides and Trace Elements. IAEATECDC-1360. IAEA, Vienna.
- Kalfas CA, Axiotis M, Tsabaris C (2016) SPECTRW: A software package for nuclear and atomic spectroscopy. *Nucl Inst Methods Phys Res A* 830:265–274. <https://doi.org/10.1016/j.nima.2016.05.098>
- Karageorgis AP, Anagnostou CL, Kaberi H (2005) Geochemistry and mineralogy of the NW Aegean Sea surface sediments: implications for river runoff and anthropogenic impact. *Appl Geochem* 20:69–88. <https://doi.org/10.1016/j.apgeochem.2004.07.008>
- Karageorgis AP, Katsanevakis S, Kaberi H (2009) Use of enrichment factors for the assessment of heavy metal contamination in the sediments of Koumoundourou Lake, Greece. *Water Air Soil Pollut* 204: 243–258. <https://doi.org/10.1007/s11270-009-0041-9>
- Kelepertzis A, Argyraki A, Alexakis D (2006) Multivariate statistics and spatial interpretation of geochemical data for assessing soil contamination by potentially toxic elements in the mining area of Stratoni, north Greece. *Geochem Explor Environ A* 6:349–355. <https://doi.org/10.1144/1467-7873/05-101>
- Kelepertzis E (2013) Heavy metals baseline concentrations in soft tissues of Patell sp. from the Stratoni coastal environment, NE Greece. *Ecol Chem Eng S* 20:141–149. <https://doi.org/10.2478/eces-2013-0011>
- Kelepertzis E, Argyraki A, Daftsis E (2012) Geochemical signature of surface water and stream sediments of a mineralized drainage basin at NE Chalkidiki, Greece: a pre-mining survey. *J Geochem Explor* 114:70–81. <https://doi.org/10.1016/j.gexplo.2011.12.006>
- Lazaridou-Dimitriadou M, Koukoumides C, Lekka E, Gaidagis G (2004) Integrative evaluation of the ecological quality of metalliferous streams (Chalkidiki, Macedonia, Hellas). *Environ Monit Assess* 90:59–86. <https://doi.org/10.1023/B:EMAS.0000009230.24795.01>
- Mejjad N, Laissaoui A, El-Hammoui O, Fekri A, Amsil H, El-Yahyaoui A, Benkdad A (2018) Geochemical, radiometric, and environmental approaches for the assessment of the intensity and chronology of metal contamination in the sediment cores from Oualidia lagoon (Morocco). *Environ Sci Pollut Res* 25:22872–22888. <https://doi.org/10.1007/s11356-018-2370-y>

- Noli F, Tsamos P (2018) Seasonal variations of natural radionuclides, minor and trace elements in lake sediments and water in a lignite mining area of North-Western Greece. *Environ Sci Pollut Res* 25: 12222–12233. <https://doi.org/10.1007/s11356-017-9801-z>
- Ontario Ministry of Environment and Energy (OMEE) (1993) Guidelines for the Protection and Management of Aquatic Sediment Quality in Ontario. Ministry of Environment and Energy. ISBN0-7778-9248-7
- Paiva I, Marques R, Santos M, Reis M, Prudencio MI, Waerenborgh JC, Dias MI, Russo D, Cardoso G, Vieira BJC, Carvalho E, Rosa C, Lobarinhas D, Diamantino C, Pinto R (2019) Naturally occurring radioactive material and risk assessment of tailings of polymetallic and Ra/U mines from legacy sites. *Chemosphere* 223:171–179. <https://doi.org/10.1016/j.chemosphere.2019.02.057>
- Panagopoulos I, Karayannidis A, Adam K, Aravossis K (2009) Application of risk management techniques for the remediation of an old mining site in Greece. *Waste Manag* 29:1739–1746. <https://doi.org/10.1016/j.wasman.2008.11.017>
- Papadopoulos A, Christofides G, Koroneos A, Stoulos A, Papastefanou C (2013) Radioactive secular equilibrium in  $^{238}\text{U}$  and  $^{232}\text{Th}$  series in granitoids from Greece. *Appl Radiat Isot* 75:95–104. <https://doi.org/10.1016/j.apradiso.2013.02.006>
- Pappa FK (2018) Study and dispersion of radionuclides and heavy metals in coastal areas of Greece, characterized by active and past mining activities, National Technical University of Athens (PhD thesis-in English)
- Pappa FK, Tsabaris C, Ioannidou A, Patiris DL, Kaberi H, Pashalidis I, Eleftheriou G, Androulakaki AG, Vlastou R (2016) Radioactivity and metal concentrations in marine sediments associated with mining activities in Ierissos Gulf, North Aegean Sea, Greece. *Appl Radiat Isot* 116:22–33. <https://doi.org/10.1016/j.apradiso.2016.07.006>
- Pappa FK, Tsabaris C, Patiris DL, Androulakaki EG, Eleftheriou G, Betsou C, Michalopoulou V, Kokkoris M, Vlastou R (2018) Historical trends and assessment of radionuclides and heavy metals in sediments near an abandoned mine, Lavrio, Greece. *Environ Sci Pollut Res* 1-17. <https://doi.org/10.1007/s11356-018-2984-0>
- Pappa FK, Tsabaris C, Patiris DL, Androulakaki EG, Ioannidou A, Eleftheriou G, Kokkoris M, Vlastou R (2019) Dispersion pattern of  $^{226}\text{Ra}$  and  $^{235}\text{U}$  using the ERICA Tool in the coastal mining area, Ierissos Gulf, Greece. *Appl Radiat Isot* 145:198–204. <https://doi.org/10.1016/j.apradiso.2018.12.021>
- Patiris DL, Tsabaris C, Anagnostou CL, Androulakaki EG, Pappa FK, Eleftheriou G, Sgouros G (2016) Activity concentration and spatial distribution of radionuclides in marine sediments close to the estuary of Shatt al-Arab/Arvand Rud River, the Gulf. *J Environ Radioact* 157:1–15. <https://doi.org/10.1016/j.jenvrad.2016.02.025>
- Pavlovic G, Barisic D, Lovrencic I, Orescanin V, Prohic E (2005) Use of fallout  $^{137}\text{Cs}$  for documenting the chronology of overbank sediments from the river Sava, Croatia, and interpreting their geochemical patterns. *Environ Geol* 47:475–481. <https://doi.org/10.1007/s00254-004-1167-0>
- Persianis D, Katsikis J, Karageorgiou DE (2010) The genetic hypothesis of the uraniferous mineralization, eastern Chalkidiki (Northern Greece). *Bulletin of the Geological Society of Greece, Proceedings of the 12<sup>th</sup> international congress*, Patra
- Riba I, DelValls TA, Forja JM, Gomez-Parra A (2002) Influence of the Aznalcollar mining spill on the vertical distribution of heavy metals in sediments from the Guadalquivir estuary (SW Spain). *Mar Pollut Bull* 44:39–47. [https://doi.org/10.1016/S0025-326X\(01\)00171-0](https://doi.org/10.1016/S0025-326X(01)00171-0)
- Ruiz-Fernandez AC, Hillaire-Marcel C (2009)  $^{210}\text{Pb}$ -derived ages for the reconstruction of terrestrial contaminant history into the Mexican Pacific coast: potential and limitations. *Mar Pollut Bull* 59:134–145. <https://doi.org/10.1016/j.marpollbul.2009.05.006>
- Salomons W, Forstner U (1984) *Metals in the Hydrocycle*. Springer-Verlag, Berlin
- Stamatis N, Ioannidou D, Christoforidis A, Koutrakis E (2002) Sediment pollution by heavy metals in the Strymonikos and Ierissos Gulfs, North Aegean Sea, Greece. *Environ Monit Assess* 80:33–49
- Szarlowicz K, Reczynski W, Misiak R, Kubica B (2013) Radionuclides and heavy metal concentrations as complementary tools for studying the impact of industrialization on the environment. *J Radioanal Nucl Chem* 298:1323–1333. <https://doi.org/10.1007/s10967-013-2548-1>
- Tomlinson DL, Wilson JG, Harris CR, Jeffrey DW (1980) Problems in the assessment of heavy-metal levels in estuaries and the formation of a pollution index. *Helgoländer Meeresun* 33:566–575
- Tsabaris C, Eleftheriou G, Kapsimalis V, Anagnostou C, Vlastou R, Durmishi C, Kedhi M, Kalfas CA (2007) Radioactivity levels of recent sediments in the Butrint Lagoon and the adjacent coast of Albania. *Appl Radiat Isot* 65:445–453. <https://doi.org/10.1016/j.apradiso.2006.11.006>
- Tsabaris C, Evangelidou N, Fillis E, Sotiropoulou M, Patiris DL, Florou H (2012) Distribution of natural radioactivity in sediment cores from Amvrakikos Gulf 26 (Western Greece) as part of IAEA's campaign in Adriatic and Ionian Seas. *Radiat Prot Dosim* 150:474–487. <https://doi.org/10.1093/rpd/ncr436>
- Tzamos E, Papadopoulos A, Grieco G, Stoulos S, Bussolesi M, Daftsis E, Vagli E, Dimitriadis D, Godelitsas A (2019) Investigation of trace and critical elements (including actinides) in flotation sulphide concentrates of Kassandra Mines (Chalkidiki, Greece). *Geosciences* 9: 164. <https://doi.org/10.3390/geosciences9040164>
- United Nations Scientific Committee on the Effects of Atomic Radiation (UNSCEAR) (2000) Sources and Effects of Ionizing Radiation, United Nations Scientific Committee on the Effects of Atomic Radiation. Report to General Assembly with Scientific Annexes, United Nations, New York
- United States Environmental Protection Agency (USEPA) (2000) Prediction of sediment toxicity using consensus-based freshwater sediment quality guidelines, EPA 905/R-00/007, June 2000
- Vaalgamaa S, Korhola A (2007) Geochemical signatures of two different coastal depositional environments within the same catchment. *J Paleolimnol* 38:241–260. <https://doi.org/10.1007/s10933-006-9071-0>
- Valette-Silver NJ (1993) The use of sediment core to reconstruct historical trends in contamination of estuarine and coastal sediments. *Estuaries* 16(3B):577–588. <https://doi.org/10.2307/1352796>
- Wang S, Wang Y, Zhang R, Wang W, Xu D, Guo J, Li P, Yu K (2015) Historical levels of heavy metals reconstructed from sedimentary record in the Hejiang River, located in a typical mining region of Southern China. *Sci Total Environ* 532:645–654. <https://doi.org/10.1016/j.scitotenv.2015.06.035>
- Wedepohl KH (1995) The composition of the continental crust. *Geochim Cosmochim Acta* 59(7):1217–1232. [https://doi.org/10.1016/0016-7037\(95\)00038-2](https://doi.org/10.1016/0016-7037(95)00038-2)
- Wennrich R, Mattusch J, Morgenstem P, Freyer K, Treutler HC, Stark HJ, Bruggemann L, Paschke A, Daus B, Weiss H (2004) Characterization of sediments in an abandoned mining area; a case study of Mansfeld region, Germany. *Environ Geol* 45:818–833. <https://doi.org/10.1007/s00254-003-0942-7>
- Yao S, Xue B (2014) Heavy metal records in the sediments of Nanyihu Lake, China: influencing factors and source identification. *J Paleolimnol* 51:15–27. <https://doi.org/10.1007/s10933-013-9752-4>
- Yao S, Xue B (2016) Sediment records of the metal pollution at Chihu Lake near a copper mine at the middle Yangtze River in China. *J Limnol* 75(1):121–134. <https://doi.org/10.4081/jlimnol.2015.1241>
- Zeng H, Wu J (2009) Sedimentary records of heavy metal pollution in Fuxian Lake, Yunnan Province, China: intensity, history, and sources. *Pedosphere* 19(5):562–569. [https://doi.org/10.1016/S1002-0160\(09\)60150-8](https://doi.org/10.1016/S1002-0160(09)60150-8)